Algerian Journal of Research and Technology
AJRTDZ@gmail.com
http://www.univ-usto.dz/AJRT/

ISSN : 2543-3954 *A.J.R.T Volume 2 (N° 1) (2018) 54-69*

Analysis of Bending of Functionally Graded Plates with Porosities Using of High Order Shear Theory

Merdaci Slimane[a,*]

[a] *Structures and Advanced Materials in Civil Engineering and Public Works Laboratory, University of Sidi Bel Abbes, Faculty of Technology, Civil Engineering and Public Works Department, Algeria.*

[*]*Corresponding author.* slimanem2016@gmail.com

Abstract. This work consists of the analysis of the bending responses of porous functionally graded (FG) rectangular plates according to high order shear deformation theory. The proposed theory contains four unknowns unlike the other theories which contain five unknowns, but it checks the boundary conditions without constraints on the upper and lower plate surfaces. Both the effect of shear strain and normal deformation are included in the present theory and so it does not need any shear correction factor. The equilibrium equations according to the porous FG plates are derived. The solution of the problem is derived by using Navier's technique. Numerical results have been reported, and compared with those available in the open literature for non-porous plates. Effects of the exponent graded and porosity factors are investigated.

Keywords: functionally graded; rectangular plates; porosity; high order theory, shear-deformation.

INTRODUCTION

Functionally graded materials (FGMs) are known for their tailor-made properties which are achieved through the continuous gradation of material phase from one surface to another. Due to FGMs being involved in the classification of composite materials, the material compositions of FGMs are assumed to vary smoothly and continuously throughout the gradient directions. The earliest FGMs were introduced by Japanese scientists in the mid-1980s as ultra-high temperature resistant materials for aerospace applications. Recently, these materials have found other uses in electrical devices, energy transformation, biomedical engineering, optics, etc. (Suresh, 1998). At the introduction of FGMs, most of the essential concepts and information about the materials were largely unknown outside of Japan. However, in the manufacture of FGM, porosities may occur in the materials during the sintering process. This is due to the large difference in coagulation temperature between the components of the material (Zhu, 2001). Wattanasakulpong et al. (2012) discussed the porosities that occur in lateral FGM samples made with a multistage sequential filtration technique. So, it is important to take under consideration the porosity effect when designing FG components under the effect of dynamic loadings.

On the basis of open literature, it seems that many investigators have paid their attentions on discussing analyses of FGM structures with porosities. Most of these investigations are concerned with vibration behavior of FG porous structures (Rezaei, 2015; Behravan, 2015; Rezaei, 2016; Shafiei, 2016; Chen, 2016; Ebrahimi, 2016; Shafiei, 2017; Ebrahimi, 2017; Rezaei, 2017; Rezaei, 2017; Lhoucine, 2017; Wang, 2017; Ghadiri, 2017; Al Rjoub, 2017; Ghorbanpour, 2017; Barati, 2017; Wu, 2018; Arshid, 2018; Chen, 2018; Li, 2018; Barati, 2018; Ebrahimi, 2018). Additional researchers are restricted their attention to the buckling (Jabbari, 2014; Khorshidvand, 2014; Mojahedin, 2014; Farzaneh, 2015; Barati, 2016; Mojahedin, 2016; Feyzi, 2017; Rezaei, 2017; Cong, 2018) or vibration and buckling (Shojaeefard, 2017; Chen, 2017; Kitipornchai, 2017; Yang, 2018) of many porous structures.

In the past three decades, researches on plates have received great attention, and a variety of plate theories has been proposed, in which the plates are generally subjected to various types of mechanical loads. In particular, knowledge pertaining to bending is essential for optimal design of structures. For example, our numerical examples clearly show that with a suitable volume fraction exponent "P" for FGM, one could achieve an optimal design for FGM plates.

It is worthwhile to present some developments in the plate theory. The classical plate theory (CPT), which neglects the transverse shear effects, provides reasonable results for thin plates; however, it underpredicts deflections and overpredicts frequencies as well as buckling loads for moderately thick plates. For composite plates and shells, the shear deformation, extensional-bending and bending-shear couplings play important role in the failure and instability of structures (Zhang, 1991; Zhang, 1994; Shen, 1990). Therefore, in order to obtain accurate and reliable predictions of responses of composite plates, it is necessary to develop a new engineering theory. Many shear deformation theories accounting for transverse shear effects have been developed to overcome the deficiencies of the CPT. The first-order shear deformation theories (FSDPTs) based on Reissner and Mindlin accounted for the transverse shear effects bymeans of linear variation of in-plane displacements across the thickness. Since FSDPT violates the equilibrium conditions at the plate's top and bottom faces, the shear correction factors are needed to rectify the unrealistic variation of the shear strain/stress across the thickness. In order to overcome the limitations of FSDPT, higher-order shear deformation theories (HSDPTs) involving higher-order terms in Taylor's expansions of the displacements in the thickness coordinate were developed. A good review of these theories for the analysis of laminated composite plates. Recently, a two variable refined plate theory was developed by (Kim et al., 2009) for laminated composite plates, the most interesting feature of which is that it does not require shear correction factor, and has strong similarities to the CPT in such respects as governing equation, boundary conditions and moment expressions.

The objective of this article is to present the bending behavior of FG plates having porosities. The plate may be either perfectly porous homogeneous or has a perfect homogeneity shape according to the values of the volume fraction of voids (porosity) or the graded factors. The plate is assumed isotropic at any point within the plate, with its Young's modulus varying across its thickness in accord with a power-law in terms of the volume fractions of the plate constituents while the poisson's ratio remaining constant. The present theory satisfies equilibrium conditions at the plate's top and bottom faces without using shear correction factors. Navier solution is used to obtain closed-form solutions for simply supported FG plates. Several important aspects, i.e., aspect ratios, thickness ratios, exponent graded factor as well as porosity volume fraction, which affect deflections and stresses, are taken into investigation.

FORMULATION OF THE PROBLEM

Structural Model

Consider a FG thick rectangular plate of length a, width b and thickness h made of functionally graded material as shown in Fig.1 together with the adopted coordinate system. The material properties of the FG plate, such as Young's modulus E, are assumed to be function of the volume fraction of constituent materials.

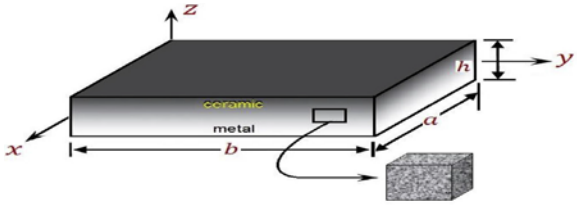

Fig. 1. Geometry and coordinates of the FG porous plate.

Let the FGM plate be subjected to a transverse load *q(x,y)*, and a rectangular Cartesian coordinate of x and y is introduced for the deformation analysis of the plate. The plate under study is bounded by the co-ordinate planes x = 0, a and y = 0, b. The reference surface is the middle surface of the plate defined by z =0, and z denotes the thickness co-ordinate measured from the un-deformed middle surface. Let the present plate is converted from lower to upper surfaces according to an exponential or polynomial laws. We will consider firstly a non-homogeneity material with a porosity volume function, α ($0 \leq \alpha \leq 1$). In such a way, the efficient material properties, as Young's modulus, can be expressed as:

$$E = E_0 e^{\left(\frac{1}{2}-\frac{z}{h}\right)^P - \frac{2\alpha}{1-\alpha}} \quad (1)$$

where P ($P \geq 0$) represents a factor that points out the material variation through the thickness. Note that the plate is perfectly porous homogeneous when k equals zero and it gets the perfect homogeneity shape when P = α = 0.

The functional relationship between E(z) for the ceramic and metal FGM plate is assumed to

$$E(z) = E_m\left(1 - V - \frac{\alpha}{2}\right) + E_c\left(V - \frac{\alpha}{2}\right)$$

And:

$$V = \left(\frac{1}{2} - \frac{z}{h}\right)^p \quad (2)$$

where E_c and E_m are the corresponding properties of the ceramic and metal, respectively, and "P" is the volume fraction exponent which takes values greater than or equal to zero. The above power-law assumption reflects a simple rule of mixtures used to obtain the effective properties of the ceramic-metal plate. The rule of mixtures applies only to the thickness direction. Note that the volume fraction of the metal is high near the bottom surface of the plate, and that of the ceramic is high near the top surface. Furthermore, Eq. (2) indicates that the bottom surface of the plate (z = −h/2) is metal whereas the top surface (z = h/2) of the plate is ceramic.

Assumptions of the Present Plate Theory

- The displacements are small in comparison with the plate thickness, and, therefore, strains involved are infinitesimal.
- The transverse displacement w includes two components of bending w_b, and shear w_s. These components are functions of coordinates x, y only.

$w(x, y, z) = w_b(x, y) + w_s(x, y)$ (3)

- The transverse normal stress $\boldsymbol{\sigma_z}$ is negligible in comparison with in-plane stresses σx and $\boldsymbol{\sigma_y}$.
- The displacements u in x-direction and v in y-direction consist of extension, bending, and shear components.

$U = u_0 + u_b + u_s$, $V = v_0 + v_b + v_s$ (4)

The bending components ub and vb are assumed to be similar to the displacements given by the classical plate theory. Therefore, the expression for ub and vb can be given as

$$u_b = -z\frac{\partial w_b}{\partial x} \quad (5)$$

$$v_b = -z\frac{\partial w_b}{\partial y}$$

The shear components « u_s» and «n_s» give rise, in conjunction with «w_s», to the parabolic variations of shear strains «g_{xz}»,«g_{yz}» and hence to shear stresses «t_{xz}», « t_{yz}» through the thickness of the plate in such a way that shear stresses «t_{xz}», « t_{yz}» are zero at the top and bottom faces of the plate. Consequently, the expression for «u_s» and «v_s»can be given as

$$u_s = -f(z)\frac{\partial w_s}{\partial x} \quad (6)$$

$$v_s = -f(z)\frac{\partial w_s}{\partial y}$$

DISPLACEMENT FIELD AND CONSTITUTIVE EQUATIONS

In the present analysis, the shear deformation plate theory is suitable for the displacements (Merdaci et al 2009).

$$\begin{aligned} u(x,y,z) &= u_0(x,y) - z\frac{\partial w_b}{\partial x} - f(z)\frac{\partial w_s}{\partial x} \\ v(x,y,z) &= v_0(x,y) - z\frac{\partial w_b}{\partial y} - f(z)\frac{\partial w_s}{\partial y} \\ w(x,y,z) &= w_b(x,y) + w_s(x,y) \end{aligned} \quad (7)$$

Note that the displacement field of the classical plate theory (CPT) will be given by setting $f(z) = 0$, first-order shear deformation theory (FSDPT) will be given by setting $f(z) = z$ .However, the displacement fields of the higher-order (HSDPT) , exponential (ESDPT) and sinusoidal (SSDPT) plate theories will be given, respectively, by setting:

$$f(z) = z\left(1 - \frac{4z^2}{3h^2}\right), \quad f(z) = z.e^{-2(z/h)^2}$$

And

$$f(z) = \frac{h}{\pi}sin\left(\frac{\pi z}{h}\right)$$

However, in the present theory one considers a new perception of f(z) (Merdaci et al 2009) as:

$$f(z) = z - \frac{h}{\pi}\sin\left(\frac{\pi z}{h}\right) \quad (8)$$

The strains associated with the displacements in Eq. (8) are:

$$\begin{aligned} \varepsilon_x &= \varepsilon_x^0 + z\,k_x^b + f(z)\,k_x^s \\ \varepsilon_y &= \varepsilon_y^0 + z\,k_y^b + f(z)\,k_y^s \\ \gamma_{xy} &= \gamma_{xy}^0 + z\,k_{xy}^b + f(z)\,k_{xy}^s \\ \gamma_{yz} &= g(z)\,\gamma_{yz}^s \\ \gamma_{xz} &= g(z)\,\gamma_{xz}^s \\ \varepsilon_z &= 0 \end{aligned} \quad (9)$$

where

$$\varepsilon_x^0 = \frac{\partial u_0}{\partial x}$$

$$k_x^b = -\frac{\partial^2 w_b}{\partial x^2}$$

$$k_x^s = -\frac{\partial^2 w_s}{\partial x^2}$$

$$\varepsilon_y^0 = \frac{\partial v_0}{\partial y}$$

$$k_y^b = -\frac{\partial^2 w_b}{\partial y^2}$$

$$k_y^s = -\frac{\partial^2 w_s}{\partial y^2} \quad (10)$$

$$\gamma_{xy}^0 = \frac{\partial u_0}{\partial y} + \frac{\partial v_0}{\partial x}$$

$$k_{xy}^b = -2\frac{\partial^2 w_b}{\partial x \partial y}$$

$$k_{xy}^s = -2\frac{\partial^2 w_s}{\partial x \partial y}$$

$$\gamma_{yz}^s = \frac{\partial w_s}{\partial y}$$

$$\gamma_{xz}^s = \frac{\partial w_s}{\partial x} \quad g(z) = 1 - f'(z)$$

$$f'(z) = \frac{df(z)}{dz}$$

For elastic and isotropic FGMs, the constitutive relations can be written as

$$\begin{Bmatrix} \sigma_x \\ \sigma_y \\ \tau_{xy} \end{Bmatrix} = \begin{bmatrix} Q_{11} & Q_{12} & 0 \\ Q_{12} & Q_{22} & 0 \\ 0 & 0 & Q_{66} \end{bmatrix} \begin{Bmatrix} \varepsilon_x \\ \varepsilon_y \\ \gamma_{xy} \end{Bmatrix}$$

$$\begin{Bmatrix} \tau_{yz} \\ \tau_{zx} \end{Bmatrix} = \begin{bmatrix} Q_{44} & 0 \\ 0 & Q_{55} \end{bmatrix} \begin{Bmatrix} \gamma_{yz} \\ \gamma_{zx} \end{Bmatrix} \quad (11)$$

where (σ_x, σ_y, τ_{xy}, τ_{yz}, τ_{yx}) and (ε_x, ε_y, γ_{xy}, γ_{yz}, γ_{yx}) are the stress and strain components, respectively. Using the material properties defined in Eq.(1), the stiffness coefficients, Q_{ij}, can be expressed as

$$Q_{11} = Q_{22} = \frac{E(z)}{1-\nu^2},$$

$$Q_{12} = \frac{\nu E(z)}{1-\nu^2}, \quad (12)$$

$$Q_{44} = Q_{55} = Q_{66} = \frac{E(z)}{2(1+\nu)},$$

EQUILIBRIUM EQUATIONS

The static equations can be obtained by using the principle of virtual displacements. It can be stated in its analytical form as

$$\int_{-h/2}^{h/2}\int_{\Omega}\left[\sigma_x\delta\varepsilon_x+\sigma_y\delta\varepsilon_y+\tau_{xy}\delta\gamma_{xy}+\tau_{yz}\delta\gamma_{yz}+\tau_{xz}\delta\gamma_{xz}\right]d\Omega\,dz-\int_{\Omega}q\delta W\,d\Omega=0 \tag{13}$$

where Ω is the top surface.

By substituting Eqs. (10) and (11) into Eq. (13) and integrating through the thickness of the plate, Eq. (14) can be rewritten as

$$\int_{\Omega}\left[N_x\delta\varepsilon_x^0+N_y\delta\varepsilon_y^0+N_{xy}\delta\varepsilon_{xy}^0+M_x^b\delta k_x^b+M_y^b\delta k_y^b+M_{xy}^b\delta k_{xy}^b+M_x^s\delta k_x^s+M_y^s\delta k_y^s+M_{xy}^s\delta k_{xy}^s+S_{yz}^s\delta\gamma_{yz}^s+S_{xz}^s\delta\gamma_{xz}^s\right]$$
$$d\Omega-\int_{\Omega}q\left(\delta w_b+\delta ws\right)d\Omega=0 \tag{14}$$

Where the stress resultants N, M, and S are defined by:

$$\left\{N_x,N_y,N_{xy}\right\}=\int_{-h/2}^{h/2}\left(\sigma_x,\sigma_y,\tau_{xy}\right)dz,$$

$$\left\{M_x^b,M_y^b,M_{xy}^b\right\}=\int_{-h/2}^{h/2}\left(\sigma_x,\sigma_y,\tau_{xy}\right)zdz,\qquad \left(S_{xz}^s,S_{yz}^s\right)=\int_{-h/2}^{h/2}\left(\tau_{xz},\tau_{yz}\right)g(z)dz. \tag{15}$$

$$\left\{M_x^s,M_y^s,M_{xy}^s\right\}=\int_{-h/2}^{h/2}\left(\sigma_x,\sigma_y,\tau_{xy}\right)f(z)dz,$$

By substituting Eq. (11) into Eq. (15) and integrating through the thickness of the plate, the stress resultants are given as:

$$\begin{Bmatrix}\boldsymbol{N}\\ \boldsymbol{M}^b\\ \boldsymbol{M}^s\end{Bmatrix}=\begin{bmatrix}\boldsymbol{A}&\boldsymbol{B}&\boldsymbol{B}^s\\ \boldsymbol{A}&\boldsymbol{D}&\boldsymbol{D}^s\\ \boldsymbol{B}^s&\boldsymbol{D}^s&\boldsymbol{H}^s\end{bmatrix}\begin{Bmatrix}\boldsymbol{\varepsilon}\\ \boldsymbol{k}^b\\ \boldsymbol{k}^s\end{Bmatrix},\quad \boldsymbol{S}=\boldsymbol{A}^s\boldsymbol{\gamma}, \tag{16}$$

$$\boldsymbol{N}=\left\{N_x,N_y,N_{xy}\right\}^t,\ \boldsymbol{M}^b=\left\{M_x^b,M_y^b,M_{xy}^b\right\}^t,\ \boldsymbol{M}^s=\left\{M_x^s,M_y^s,M_{xy}^s\right\}^t, \tag{17a}$$

$$\boldsymbol{\varepsilon}=\left\{\varepsilon_x^0,\varepsilon_y^0,\gamma_{xy}^0\right\}^t,\ \boldsymbol{k}^b=\left\{k_x^b,k_y^b,k_{xy}^b\right\}^t,\ \boldsymbol{k}^s=\left\{k_x^s,k_y^s,k_{xy}^s\right\}^t, \tag{17b}$$

$$\boldsymbol{A}=\begin{bmatrix}A_{11}&A_{12}&0\\ A_{12}&A_{22}&0\\ 0&0&A_{66}\end{bmatrix},\quad \boldsymbol{B}=\begin{bmatrix}B_{11}&B_{12}&0\\ B_{12}&B_{22}&0\\ 0&0&B_{66}\end{bmatrix},\quad \boldsymbol{D}=\begin{bmatrix}D_{11}&D_{12}&0\\ D_{12}&D_{22}&0\\ 0&0&D_{66}\end{bmatrix}, \tag{17c}$$

$$\boldsymbol{B}^s=\begin{bmatrix}B_{11}^s&B_{12}^s&0\\ B_{12}^s&B_{22}^s&0\\ 0&0&B_{66}^s\end{bmatrix},\quad \boldsymbol{D}^s=\begin{bmatrix}D_{11}^s&D_{12}^s&0\\ D_{12}^s&D_{22}^s&0\\ 0&0&D_{66}^s\end{bmatrix},\quad \boldsymbol{H}^s=\begin{bmatrix}H_{11}^s&H_{12}^s&0\\ H_{12}^s&H_{22}^s&0\\ 0&0&H_{66}^s\end{bmatrix} \tag{17d}$$

$$\boldsymbol{S}=\left\{S_{xz}^s,S_{yz}^s\right\}^t,\quad \boldsymbol{\gamma}=\left\{\gamma_{xz},\gamma_{yz}\right\}^t,\quad \boldsymbol{A}^s=\begin{bmatrix}A_{44}^s&0\\ 0&A_{55}^s\end{bmatrix}, \tag{17e}$$

where *Aij* , *Bij* , etc. are the plate stiffness defined by

$$\left\{A_{11},B_{11},D_{11},B_{11}^s,D_{11}^s,H_{11}^s\right\}=\int_{-h/2}^{h/2}Q_{11}*1\left(1,z,z^2,f(z),z\,f(z),f^2(z)\right)dz,$$

$$\left\{A_{12},B_{12},D_{12},B_{12}^s,D_{12}^s,H_{12}^s\right\}=\int_{-h/2}^{h/2}Q_{11}*v*\left(1,z,z^2,f(z),z\,f(z),f^2(z)\right)dz, \tag{18a}$$

$$\left\{A_{66},B_{66},D_{66},B_{66}^s,D_{66}^s,H_{66}^s\right\}=\int_{-h/2}^{h/2}Q_{11}*\frac{1-v}{2}*\left(1,z,z^2,f(z),z\,f(z),f^2(z)\right)dz,$$

$$\left(\boldsymbol{A}_{22},\boldsymbol{B}_{22},\boldsymbol{D}_{22},\boldsymbol{B}_{22}^s,\boldsymbol{D}_{22}^s,\boldsymbol{H}_{22}^s\right)=\left(\boldsymbol{A}_{11},\boldsymbol{B}_{11},\boldsymbol{D}_{11},\boldsymbol{B}_{11}^s,\boldsymbol{D}_{11}^s,\boldsymbol{H}_{11}^s\right),\quad Q_{11}=\frac{E(z)}{1-v^2} \tag{18b}$$

$$A_{44}^s=A_{55}^s=\int_{-h/2}^{h/2}\frac{E(z)}{2(1+v)}\left[g(z)\right]^2dz, \tag{18c}$$

The governing equations of equilibrium can be derived from Eq.(14) by integrating the displacement gradients by parts and setting the coefficients of δu, δv, δw_b, and δw_s zero separately. Thus, one can obtain the equilibrium equations associated with the present shear deformation theory,

$$\delta u: \ \frac{\partial N_x}{\partial x}+\frac{\partial N_{xy}}{\partial y}=0$$

$$\delta v: \ \frac{\partial N_{xy}}{\partial x}+\frac{\partial N_y}{\partial y}=0$$

$$\delta w_b: \ \frac{\partial^2 M_x^b}{\partial x^2}+2\frac{\partial^2 M_{xy}^b}{\partial x\partial y}+\frac{\partial^2 M_y^b}{\partial y^2}+q=0$$

$$\delta w_s: \ \frac{\partial^2 M_x^s}{\partial x^2}+2\frac{\partial^2 M_{xy}^s}{\partial x\partial y}+\frac{\partial^2 M_y^s}{\partial y^2}+\frac{\partial S_{xz}^s}{\partial x}+\frac{\partial S_{yz}^s}{\partial y}+q=0 \quad (19)$$

Substituting Eq. (16) into Eq. (19), we obtain the following equations

$$A_{11}\frac{\partial^2 u}{\partial x}+A_{66}\frac{\partial^2 u}{\partial y^2}+\left(A_{12}+A_{66}\right)\frac{\partial^2 v}{\partial x\partial y}-B_{11}\frac{\partial^3 w_b}{\partial x^3}-\left(B_{12}+2B_{66}\right)\frac{\partial^3 w_b}{\partial x\partial y^2}-\left(B_{12}^s+2B_{66}^s\right)\frac{\partial^3 w_s}{\partial x\partial y^2}-B_{11}^s\frac{\partial^3 w_s}{\partial x^3}=0, \quad (20a)$$

$$A_{22}\frac{\partial^2 v}{\partial y^2}+A_{66}\frac{\partial^2 v}{\partial y^2}+\left(A_{12}+A_{66}\right)\frac{\partial^2 u}{\partial x\partial y}-B_{22}\frac{\partial^3 w_b}{\partial y^3}-\left(B_{12}+2B_{66}\right)\frac{\partial^3 w_b}{\partial x^2\partial y}-\left(B_{12}^s+2B_{66}^s\right)\frac{\partial^3 w_s}{\partial x^2\partial y}-B_{22}^s\frac{\partial^3 w_s}{\partial y^3}=0, \quad (20b)$$

$$B_{11}\frac{\partial^3 u}{\partial x^3}+\left(B_{12}+2B_{66}\right)\frac{\partial^3 u}{\partial x\partial y^2}+\left(B_{12}+2B_{66}\right)\frac{\partial^3 v}{\partial x^2\partial y}+B_{22}\frac{\partial^3 v}{\partial y^3}-D_{11}\frac{\partial^4 w_b}{\partial x^4}-2\left(D_{12}+2D_{66}\right)\frac{\partial^4 w_b}{\partial x^2\partial y^2}$$
$$-D_{22}\frac{\partial^4 w_b}{\partial y^4}-D_{11}^s\frac{\partial^4 w_s}{\partial x^4}-2\left(D_{12}^s+2D_{66}^s\right)\frac{\partial^4 w_s}{\partial x^2\partial y^2}-D_{22}^s\frac{\partial^4 w_s}{\partial y^4}+q=0, \quad (20c)$$

$$B_{11}^s\frac{\partial^3 u}{\partial x^3}+\left(B_{12}^s+2B_{66}^s\right)\frac{\partial^3 u}{\partial x\partial y^2}+\left(B_{12}^s+2B_{66}^s\right)\frac{\partial^3 v}{\partial x^2\partial y}+B_{22}^s\frac{\partial^3 v}{\partial y^3}-D_{11}^s\frac{\partial^4 w_b}{\partial x^4}-2\left(D_{12}^s+2D_{66}^s\right)\frac{\partial^4 w_b}{\partial x^2\partial y^2}$$
$$-D_{22}^s\frac{\partial^4 w_b}{\partial y^4}-H_{11}^s\frac{\partial^4 w_s}{\partial x^4}-2\left(H_{12}^s+2H_{66}^s\right)\frac{\partial^4 w_s}{\partial x^2\partial y^2}-H_{22}^s\frac{\partial^4 w_s}{\partial y^4}+A_{55}^s\frac{\partial^2 w_s}{\partial x^2}+A_{44}^s\frac{\partial^2 w_s}{\partial y^2}+q=0 \quad (20d)$$

ANALYTICAL SOLUTIONS FOR FG PLATES

The following simply-supported boundary conditions are imposed at the side edges of the FG plate:

$$v_0=w_b=w_s=0, \quad \frac{\partial w_b}{\partial y}=\frac{\partial w_s}{\partial y}=0, \quad N_x=0, \ et \ M_x^b=M_x^s=0$$

and $x=0, a$ (21a)

$$u_0=w_b=w_s=0, \quad \frac{\partial w_b}{\partial x}=\frac{\partial w_s}{\partial x}=0, \quad N_y=0, \ et \ M_y^b=M_y^s=0$$

and $y=0, b$ (21b)

The external force according to Navier's solution can be expressed as

$$q(x,y)=\sum_{m=1}^{\infty}\sum_{n=1}^{\infty}q_{mn}\sin(\lambda x)\sin(\mu y) \quad (22)$$

Where, $\lambda=m\pi/a$ and $\mu=n\pi/b$, « m » and « n »are mode numbers. For the case of a sinusoidally distributed load, we have

$m=n=1$, et $q_{11}=q_0$ (23)

Where, q0 represents the intensity of the load at the plate center.

Following the Navier solution procedure, we assume the following form of solution for (u, v, w_b, w_s) that satisfies the boundary conditions

$$\begin{Bmatrix} u \\ v \\ w_b \\ w_s \end{Bmatrix} = \begin{Bmatrix} U_{mn}\cos(\lambda x)\sin(\mu y) \\ V_{mn}\sin(\lambda x)\cos(\mu y) \\ W_{bmn}\sin(\lambda x)\sin(\mu y) \\ W_{smn}\sin(\lambda x)\sin(\mu y) \end{Bmatrix}, \quad (24)$$

where U_{mn}, V_{mn},W_{bmn}, *a*nd W_{smn} are arbitrary parameters. Eq.(14) in combination with Eq. (19) can be combined into a system of first order equations as:

$$[K]\{\Delta\} = \{F\}, \quad (25)$$

Where, $\{\Delta\}$ and $\{F\}$ denotes the columns

$$\{\Delta\}^T = \{U_{mn}, V_{mn}, W_{bmn}, W_{smn}\}, \text{ and } \{F\}^T = \{0, 0, -q_{mn}, -q_{mn}\} \quad (26)$$

And:

$$[K] = \begin{bmatrix} a_{11} & a_{12} & a_{13} & a_{14} \\ a_{12} & a_{22} & a_{23} & a_{24} \\ a_{13} & a_{23} & a_{33} & a_{34} \\ a_{14} & a_{24} & a_{34} & a_{44} \end{bmatrix} \quad (27)$$

and the elements *aij* = *aji* of the coefficient matrix [K]. The elements of the symmetric matrix [K] presented in Eq. (26) are given by

$$\begin{aligned}
a_{11} &= -\left(A_{11}\lambda^2 + A_{66}\mu^2\right) \\
a_{12} &= -\lambda\mu\left(A_{12} + A_{66}\right) \\
a_{13} &= \lambda[B_{11}\lambda^2 + (B_{12} + 2B_{66})\mu^2] \\
a_{14} &= \lambda[B^s_{11}\lambda^2 + (B^s_{12} + 2B^s_{66})\mu^2] \\
a_{22} &= -\left(A_{66}\lambda^2 + A_{22}\mu^2\right) \\
a_{23} &= \mu[(B_{12} + 2B_{66})\lambda^2 + B_{22}\mu^2] \\
a_{24} &= \mu[(B^s_{12} + 2B^s_{66})\lambda^2 + B^s_{22}\mu^2] \quad (28) \\
a_{33} &= -\left(D_{11}\lambda^4 + 2(D_{12} + 2D_{66})\lambda^2\mu^2 + D_{22}\mu^4\right) \\
a_{34} &= -\left(D^s_{11}\lambda^4 + 2(D^s_{12} + 2D^s_{66})\lambda^2\mu^2 + D^s_{22}\mu^4\right) \\
a_{44} &= -\left(H^s_{11}\lambda^4 + 2(H^s_{12} + 2H^s_{66})\lambda^2\mu^2 + H^s_{22}\mu^4 + A^s_{55}\lambda^2 + A^s_{44}\mu^2\right)
\end{aligned}$$

NUMERICAL RESULTS AND DISCUSSIONS

In this section, the present refined theory is applied to the bending analysis of FG plates. The Poisson's ratio is fixed at ν = 0.3, and comparisons are made with available solutions. Numerical case studies are used to verify the accuracy of the present analysis. The FG plate is taken to be made of aluminum and alumina with the following material properties:

- Metal (Aluminum, Al): Em = 70 GPa; ν = 0.3.
- Ceramic (Alumina, Al_2O_3): Ec = 380 GPa; ν = 0.3.

The various non-dimensional parameters used are:

$$\bar{w} = \frac{10hE_0}{a^2 q_0} w\left(\frac{a}{2}, \frac{b}{2}\right)$$

$$\bar{\sigma}_x = \frac{10h^2}{a^2 q_0}\sigma_x\left(\frac{a}{2}, \frac{b}{2}, \frac{h}{2}\right)$$

$$\bar{\tau}_{xz} = \frac{h}{aq_0}\tau_{xz}\left(0, \frac{b}{2}, 0\right)$$

Thickness coordinate:

$$\bar{z} = z / h$$

As the first example, the deflections and the dimensionless stresses of the square FG plate (a/h = 10) for different values of the volume fraction P. The present predictions (present higher-order shear deformation theories) are compared with the first-order shear deformation theory (FSDPT), higher-order (HSDPT), Exponential (ESDPT) and sinusoidal (SSDPT). The inclusion of the porosity factor α is involved in Table 1, 2 and 3. The dimensionless in-plane normal stress $\bar{\sigma}_x$ and transverse normal stress $\bar{\tau}_{xz}$ are reported in Table 2 and 3. The stresses are compared with those of other theory. Generally, the present theory (with α = 0) gives a good prediction of inplane normal stress $\bar{\sigma}_x$ as compared with different models (ESDPT, HSDTT and SSDPT). However, the transverse normal stress $\bar{\tau}_{xz}$ is in good agreement with the SSDPT solution. It should be noted that all theory (FSDPT, ESDPT, HSDTT and SSDPT) were obtained on the basis of sinusoidal variation of both in-plane and transverse displacements across the thickness. It can be seen that SSDPT presented sinusoidal theory with five unknowns (Touratier, 1991). The present non-porous results (α = 0) almost more accurate than those generated by other theories. Also, the present results are compared well with those of other solution even for thicker plates. This points to the use of new assumption given in Eq. (7) has a maximal effect on the accuracy of the results. The deflection for (FSDPT, ESDPT, HSDPT and SSDPT) increases with the increase in the desired fraction, as it is found that the error percentage of FSDPT is larger compared to the other modal (ESDPT, HSDPT and SSDPT). It can be observed that the results obtained by the present models are identical to those of the sinusoidal shear deformation plate theory (SSDPT) and the higher-order shear deformation plate theory (HSDPT), respectively. In general, the fully ceramic (P=0) plates give the smallest deflections and shear stresses and the largest axial stresses. As the volume fraction exponent increases for FG plates, the deflection, axial stress, and shear stress will increase.

Table 1. Comparative study of deflections of FG plate for different volume fraction value and (α = 0).

P	FSDPT	ESDPT	HSDPT	SSDPT	Present
0	0.07791	0.07788	0.0779	0.0779	0.0779
1	0.19703	0.19597	0.19608	0.19603	0.19603
2	0.2866	0.28465	0.2849	0.28478	0.28478
3	0.3385	0.33586	0.33624	0.33606	0.33606
4	0.36737	0.36426	0.36474	0.36451	0.36451
5	38402	0.38061	0.38116	0.3809	0.3809
10	0.40768	0.40779	0.40798	0.40709	0.40702
Metal	0.41919	0.42179	0.42163	0.42172	0.4229

Table 2. Comparative study of dimensionless axial stress of FG plate for different volume fraction value and (α = 0).

P	FSDPT	ESDPT	HSDPT	SSDPT	Present
0	1.97576	1.99660	1.99432	1.99550	1.99550
1	0.93765	0.94442	0.94369	0.94407	0.94407
2	1.36934	1.37738	1.37661	1.37702	1.37702
3	1.61758	1.62625	1.62551	1.62590	1.62590

4	1.75384	1.76299	1.76229	1.76266	1.76266
5	1.83096	1.84056	1.83988	1.84025	1.84025
10	1.94563	1.95112	1.95074	1.95096	1.95702
Metal	1.97576	1.98428	1.98353	1.98392	1.99550

Table 3. Comparative study of dimensionless transverse shear stresses of FG plate for different volume fraction value and ($\alpha = 0$).

P	FSDPT	ESDPT	HSDPT	SSDPT	Present
0	0.15915	0.25379	0.23857	0.24618	0.24618
1	0.26879	0.34769	0.33432	0.34102	0.34102
2	0.34891	0.41915	0.40918	0.41426	0.41426
3	0.41002	0.47831	0.47132	0.47501	0.47501
4	0.45817	0.53051	0.52540	0.52826	0.52826
5	0.49708	0.57762	0.57336	0.57590	0.57590
10	0.61598	0.70958	0.69891	0.70450	0.75375
Metal	0.15915	0.20739	0.19984	0.20359	0.24618

Finally, additional results of deflections and stresses are reported in tables 4, 5 and 6 for porous FG plate ($\alpha = 0$, 0.1 and 0.2). The inclusion of porosity parameter increases the deflection and transverse shear stresses and decreases the axial stress for different values of the volume fraction graded factor P. In general, the present theory gives comparable results with the inclusion of the porosity factor (α =0, 0.1 and 0.2).It is clear that this factor has significant effect on the deflections and stresses. The inclusion of porosity parameter increases the deflection and transverse shear stresses and decreases the axial stress for different values of the volume fraction graded factor P.

Table 4. Effects of the volume fraction and porosity coefficient of deflections in a square FG-plate subjected to sinusoidally distributed load.

Theory	α	P=0	P=1	P=2	P=3	P=4	P=5	P=10	Métal
	α=0.0	0.07790	0.19604	0.28479	0.33606	0.36452	0.38090	0.40703	0.42290
Present	α=0.1	0.08122	0.21876	0.3573	0.40946	0.45243	0.47780	0.51881	0.34624
	α=0.2	0.08482	0.24749	0.40910	0.52436	0.59694	0.64172	0.71626	0.29310

Table 5. Effects of the volume fraction and porosity coefficient on the dimensionless axial stress of the FG plate.

Theory	α	P=0	P=1	P=2	P=3	P=4	P=5	P=10	Metal
	α=0.0	1.99550	0.94407	1.37702	1.62591	1.76267	1.84026	1.95703	1.99550
Present	α=0.1	1.99550	0.82120	1.26609	1.54558	1.70732	1.80177	1.94743	1.99550
	α=0.2	1.99550	0.66571	1.10626	1.41992	1.61657	1.73700	1.93093	1.99550

Table 6. Effects of volume fraction and porosity coefficient on the dimensionless transverse shear stresses in a square FG-plate subjected to sinusoidally distributed load.

Theory	α	P=0	P=1	P=2	P=3	P=4	P=5	P=10	Metal
	α=0.0	0.24618	0.34103	0.41426	0.47502	0.52827	0.57591	0.75376	0.24618
Present	α=0.1	0.24618	0.34764	0.42864	0.49672	0.55720	0.61219	0.82651	0.24618
	α=0.2	0.24618	0.35539	0.44641	0.52408	0.59391	0.65850	0.92395	0.24618

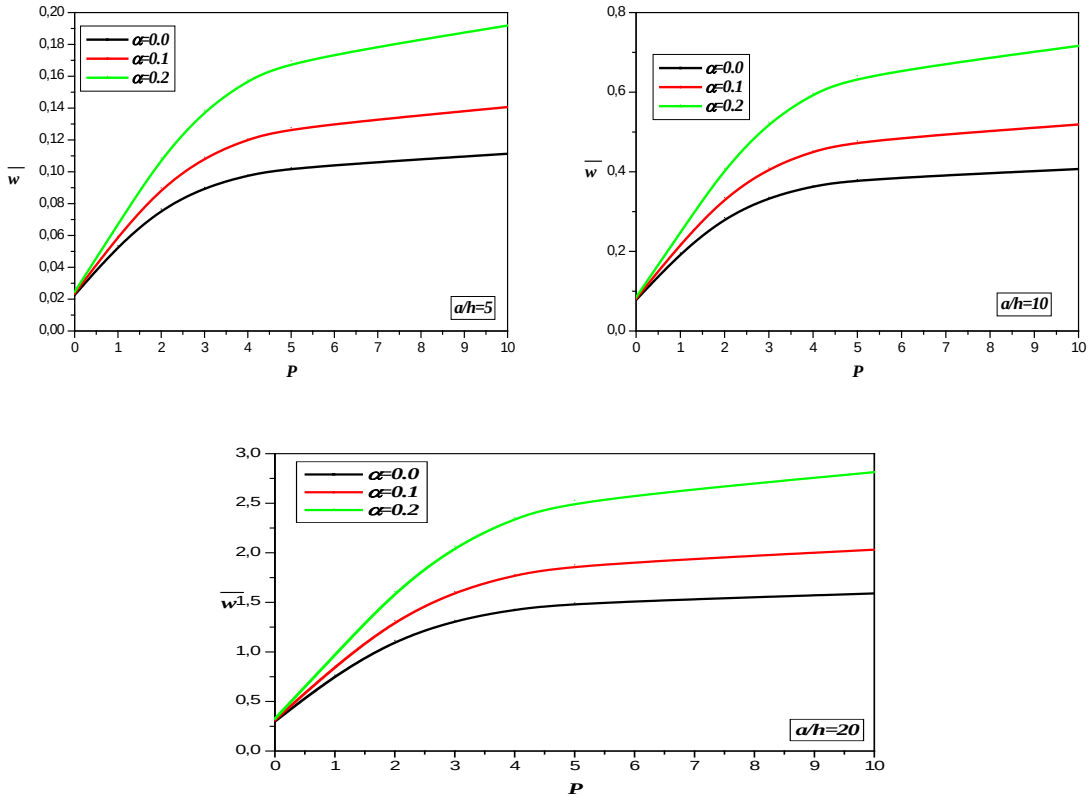

Fig.2. Displacement variation as a function of the power index "P" and the volume fraction of porosity α of a FGM plate

The effects of the material index "P" on the adimensional displacement of the perfect and imperfect FG plate for different values of the thickness ratio (a/h = 5, a/h = 10, a/h = 20) of the plate and different values of porosity coefficient using the present high order shear theory are illustrated in Figures 2 and 3 respectively. It should be noted that the dimensionless displacement increases with the increase of the value of the power law index for the perfect and imperfect FGM plate and that for the three thickness ratios. Displacements are higher for metal plates while displacements are lower for all-ceramic plates (P = 0). There is a rapid variation in displacements for the low values of the ratio a/h (that is, for a / h >20) where the plate is considered thick. Exceeding this ratio of the material index P = 3, the displacements keep a more or less constant look and this for the different values of coefficient of the porosity.

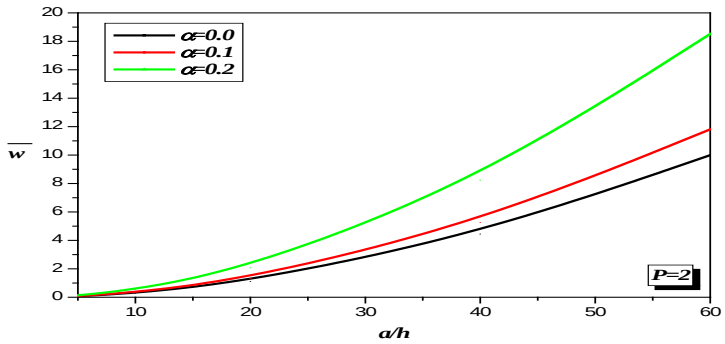

Fig.3. Variation of dimensionless displacement as a function of the thickness ratio ***a/h*** for the different values of porosity factor α.

Figure 3, shows the increase in dimensionless displacements, which is explained by the influence of material stiffness, ie an increase in the value of porosity (α), leads to a decrease in the modulus of elasticity of the material plate. An increase in the side-to-thickness ratios (a/h) leads to an increase in adimensional displacements. We can also say that the thickness ratio (a/h) has a considerable effect on dimensionless displacement.

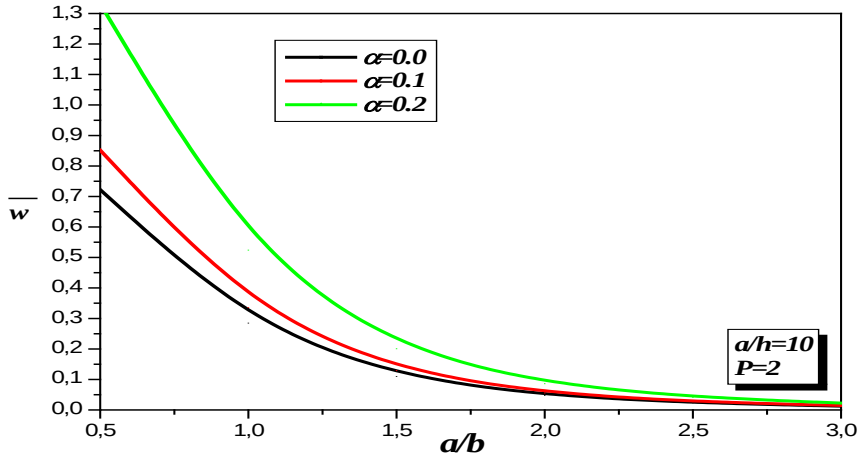

Fig.4. Variation of adimensional displacement as a function of the geometric ratio ***a/b*** for the different values of porosity factor α.

In figure 4, we study adimensional displacement variation as a function of the geometric ratio (a/b) for the different values of porosity coefficient with a ratio of equal thickness (a/h = 10) and a material index P = 2. Decreasing of said ratio makes lowering of displacement.

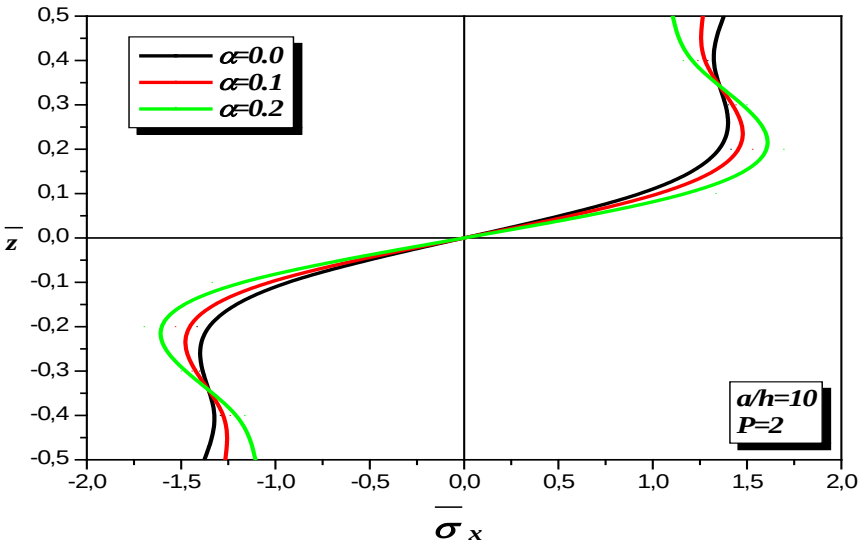

Fig.5. Through-the-thickness distribution of axial stress $\bar{\sigma}_x$ of FGM plates for different porosity factor α.

In figure 5, contains the variation of the axial stress across the plate thickness in FG. The effect of the porosity of the FGM plate was taken into account by means of the introduction of the coefficient (α). Three values are therefore retained (α = 0, 0.1, and 0.2). It can be seen that the increase in the index of porosity (α) leads to an increase in stresses. This can be justified by the fact that the porosity reduces the rigidity of the plate. The stresses are tensile above the median

plane and compression below the median plane. It is important to observe that the maximum stress depends on the value of the exponent of the volume fraction P. The in-plane normal stresses, are compressive throughout the plate up to $\bar{z} = 3.5$, and become tensile afterwards. The maximum compressive stresses occur at certain point on the bottom surface and the maximum tensile stresses occur, of course, at certain point on the top surface of the FG plate.

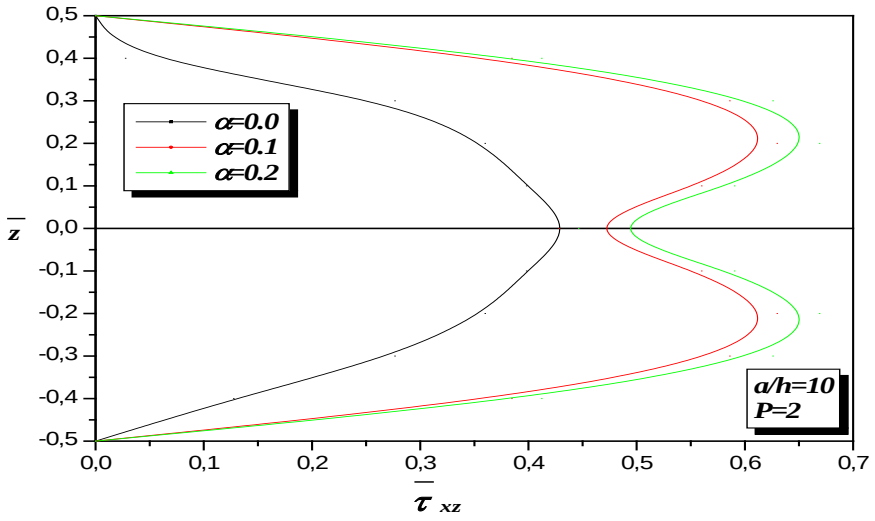

Fig.6. Through-the-thickness distribution of transverse shear stress $\bar{\tau}_{xz}$ of FGM plates for different porosity factor α.

In figure 6, shear stresses were plotted through the transverse thickness distribution. It can be seen from this figure that the porosity effect has a remarkable direct influence which occurs at a point on the median plane of the FG plate and which decreased the transverse shear stress.

CONCLUSION

A new simple theory of high order shear and normal deformation theory is developed for functionally graded plates. This theory satisfies the nullity of the shear stresses at the upper and lower surfaces of the plate without using the shear correction factor contrary to other theories. The law of the modified mixture covering the porosity phases is used to roughly describe the properties of FG-plates with porosity. The principle of virtual displacements is used to derive the governing equations and boundary conditions. Then, analytical solutions for functionally graded porous rectangular plates are presented. The inclusions of graded and porosity parameters are investigated. The effects of various parameters, such as thickness ratio, power index (exponent of the volume fraction) "***P*** ", and volume fraction of porosity on the flexion of FG plates are all discussed. Many validations examples are reported and numerical results of the present refined plate theory are accurate in predicting the bending response of non-porous plates (α=0). In addition, the present theory gave control results that can be used to evaluate various plate theories, and also to compare with the results obtained by another solution (FSDPT, ESDPT, SSDPT and HSDPT). From this work, it can be said that the present and simple theory for the resolution of the mechanical behavior of FG plates with porosity that presses manufacturing defects.

REFERENCES

Suresh S.., Mortensen A. 1998. London, Maney.
Zhu J.., Lai Z., Yin Z., Jeon J., Lee S. 2001. Mater Chem Phys. 68, 130–5.
Wattanasakulpong N., Prusty B.G., Kelly D.W., Hoffman M. 2012. Mater Des. 36, 182–90.

Rezaei AS., Saidi AR. 2015. Compos Struct. 134,1051–60.
Behravan Rad A., Shariyat M. 2015. Compos Struct. 125,558–74.
Rezaei A.S., Saidi A.R. 2016. 91,361–70.
Shafiei N., Mousavi A., Ghadiri M. 2016. Int J Eng Sci. 106,42–56.
Chen D., Yang J., Kitipornchai S. 2016. Int J Mech Sci. 108–109,14–22.
Chen D., Kitipornchai S., Yang J. Nonlinear free vibration of shear deformable sandwich beam with a functionally graded porous core. Thin-Walled Struct 2016;107,39–48.
Ebrahimi F., Ghasemi F., Salari E. Investigating thermal effects on vibration behavior of temperature-dependent compositionally graded Euler beams with porosities. Meccanica 2016;51,223–49.
Shafiei N., Mirjavadi SS., MohaselAfshari B., Rabby S., Kazemi M. Vibration of twodimensional imperfect functionally graded (2D-FG) porous nano-/micro-beams. Comput Methods Appl Mech Eng 2017;322,615–32.
Ebrahimi F., Jafari A., Barati MR. Vibration analysis of magneto-electro-elastic heterogeneous porous material plates resting on elastic foundations. Thin-Walled Struct 2017;119,33–46.
Rezaei AS., Saidi AR., Abrishamdari M., Pour Mohammadi MH. Natural frequencies of functionally graded plates with porosities via a simple four variable plate theory, an analytical approach. Thin-Walled Struct 2017;120,366–77.
Rezaei AS., Saidi AR. On the effect of coupled solid-fluid deformation on natural frequencies of fluid saturated porous plates. Eur J Mech A Solids 2017;63,99–109.
Lhoucine B., Khalid E., Rhali B. Thermal behavior analysis at large free vibration amplitudes of thin annular FGM plates with porosities. Proc Eng 2017;199,528–33.
Wang Y., Wu D. Free vibration of functionally graded porous cylindrical shell using a sinusoidal shear deformation theory. Aerosp Sci Technol 2017;66,83–91.
Ghadiri M., SafarPour H. Free vibration analysis of size-dependent functionally graded porous cylindrical microshells in thermal environment. J Therm Stresses 2017;40(1),55–71.
Al Rjoub YS., Hamad AG. Free vibration of functionally Euler-Bernoulli and Timoshenko graded porous beams using the transfer matrix method. KSCE J Civ Eng 2017;21(3),792–806.
Ghorbanpour Arani A., Khani M., Khoddami Maraghi Z. Dynamic analysis of a rectangular porous plate resting on an elastic foundation using high-order shear deformation theory. J Vib Control 2017,1–16.
Barati MR., Shahverdi H., Zenkour AM. Electro-mechanical vibration of smart piezoelectric FG plates with porosities according to a refined four-variable theory. Mech Adv Mater Struct 2017;24(12),987–98.
Wu D., Liu A., Huang Y., Huang Y., Pi Y., Gao W. Dynamic analysis of functionally graded porous structures through finite element analysis. Eng Struct 2018;165,287–301.
Arshid E., Khorshidvand AR. Free vibration analysis of saturated porous FG circular plates integrated with piezoelectric actuators via differential quadrature method. Thin-Walled Struct 2018;125,220–33.
Chen D., Kitipornchai S., Yang J. Dynamic response and energy absorption of functionally graded porous structures. Mater Des 2018;140,473–87.
Barati MR. A general nonlocal stress-strain gradient theory for forced vibration analysis of heterogeneous porous nanoplates. Eur J Mech A Solids 2018;67,215–30.
Li L., Tang H., Hu Y. Size-dependent nonlinear vibration of beam-type porous materials with an initial geometrical curvature. Compos Struct 2018;184,1177–88.
Barati MR. Vibration analysis of porous FG nanoshells with even and uneven porositydistributions using nonlocal strain gradient elasticity. Acta Mech 2018;229,1183–96.
Ebrahimi F., Jafari A. A four-variable refined shear-deformation beam theory for thermo-mechanical vibration analysis of temperature-dependent FGM beams with porosities. Mech Adv Mater Struct 2018;25(3),212–24.

Barati MR., Shahverdi H. Nonlinear vibration of nonlocal four-variable graded plates with porosities implementing homotopy perturbation and Hamiltonian methods. Acta Mech 2018;229,343–62.
Jabbari M., Mojahedin A., Haghi M. Buckling analysis of thin circular FG plates made of saturated porous-soft ferromagnetic materials in transverse magnetic field. Thin-Walled Struct 2014;85,50–6.
Khorshidvand AR., Farzaneh Joubaneh E., Jabbari M., Eslami MR. Buckling analysis of a porous circular plate with piezoelectric sensor–actuator layers under uniform radial compression. Acta Mech 2014;225,179–93.
Mojahedin A., Farzaneh Joubaneh E., Jabbari M. Thermal and mechanical stability of a circular porous plate with piezoelectric actuators. Acta Mech 2014;225,3437–52.
Jabbari M., Hashemitaheri M., Mojahedin A., Eslami MR. Thermal buckling analysisof functionally graded thin circular plate made of saturated porous materials. J Therm Stresses 2014;37,202–20.
Farzaneh Joubaneh E., Mojahedin A., Khorshidvand AR., Jabbari M. Thermal buckling analysis of porous circular plate with piezoelectric sensor-actuator layers under uniform thermal load. J Sandwich Struct Mater 2015;17(1),3–25.
Barati MR., Sadr MH., Zenkour AM. Buckling analysis of higher order graded smart piezoelectric plates with porosities resting on elastic foundation. Int J Mech Sci 2016;117,309–20.
Mojahedin A., Jabbari M., Khorshidvand AR., Eslami MR. Buckling analysis of functionally graded circular plates made of saturated porous materials based on higher order shear deformation theory. Thin-Walled Struct 2016;99,83–90.
Feyzi MR., Khorshidvand AR. Axisymmetric post-buckling behavior of saturated porous circular plates. Thin-Walled Struct 2017;112,149–58.
Rezaei AS., Saidi AR. Buckling response of moderately thick fluid-infiltrated porous annular sector plates. Acta Mech 2017;228,3929–45.
Cong PH., Chien TM., Khoa ND., Duc ND. Nonlinear thermomechanical buckling and post-buckling response of porous FGM plates using Reddy's HSDT. Aerosp Sci Technol 2018;77,419–28.
Shojaeefard MH., Googarchin HS., Ghadiri M., Mahinzare M. Micro temperaturedependent FG porous plate, free vibration and thermal buckling analysis usi modified couple stress theory with CPT and FSDT. Appl Math Model 2017;50,633–55.
Chen D., Yang J., Kitipornchai S. Nonlinear vibration and postbuckling of functionally graded graphene reinforced porous nanocomposite beams. Compos Sci Technol 2017;142,235–45.
Kitipornchai S., Chen D., Yang J. Free vibration and elastic buckling of functionally graded porous beams reinforced by graphene platelets. Mater Des 2017;116,656–65.
Yang J., Chen D., Kitipornchai S. Buckling and free vibration analyses of functionally graded graphene reinforced porous nanocomposite plates based on Chebyshev-Ritz method. Compos Struct 2018;193,281–94.
Zhang., J.W.., Shen., H.S., Postbuckling of orthotropic rectangular plates in biaxial compression. J. Eng. Mech. (ASCE) 117., 1158–1170 (1991)
Zhang., J., Investigation to the buckling and postbuckling behavior of shear-flexible plates of composite construction. Acta Mech. Sin. 26., 176–182 (in Chinese) (1994)
Shen., H., Buckling and postbuckling of moderately thick plates. Appl. Math. Mech. 11., 367–376 (in Chinese) (1990)
Kim., S.E.., Thai.,H.T.., Lee., J.,Atwo variable refined plate theory for laminated composite plates. Compos. Struct. 89., 197–205 (2009)
Praveen.,G.N.., Reddy., J.N.,Nonlinear transient thermoelastic analysis of functionally graded ceramic–metal plates. Int. J. Solids Struct. 35., 4457–4476 (1998)

Najafizadeh., M.M.., Eslami., M.R., Buckling analysis of circular plates of functionally graded materials under uniform radial compression.Int. J. Mech. Sci. 44., 2479–2493 (2002)
Merdaci S., Tounsi A., Houari MSA., Mechab I., Hebali H., Benyoucef S. Two new refined shear displacement models for functionally graded sandwich plates. Arch Appl Mech 2011;81,1507e22.
M. Touratier. An efficient standard plate theory. Engng Sci., vol. 29., no 8., pages 901-916., 1991.
A. M. Zenkour.., Kafr El-Sheikh., Thermal effects on the bending response of fiber-reinforced viscoelastic composite plates using a sinusoidal shear deformation theory., Acta Mechanica; 171 (3-4),171–187 (2004).
M. Karama.., K.S. Afaq.., S. Mistou., Mechanical behaviour of laminated composite beam by the new multi-layered laminated composite structures model with transverse shear stress continuity., Int. J. Solids Structures; 40 (6), 1525-1546., 2003.
Reissner., E., The effect of transverse shear deformation on the bending of elastic plates. J. Appl. Mech. 12., 69–77 (1945)
Mindlin., R.D., Influence of rotatory inertia and shear on flexural motions of isotropic elastic plates. J. Appl. Mech. 18.,31–38 (1951)
Reissner., E., On the theory of bending of elastic plates. J. Math. Phys. 23., 184–191 (1944)
Reddy. J.N.., Wang. C.M.., Lee. K.H. Relationships between bending solutions of classical and shear deformation beam theories. International Journal of Solids and Structures 34 (26)., 3373–338., 1997.
S.P.Timoshenko et J.M.Gere. Mechanics of Materials. New York, D.Van Nostrand Company., 1972.
Reddy J.N.., Wang., C.M., An overview of the relationships between solutions of the classical and shear deformation plate theories. Compos. Sci. Technol. 60., 2327–2335 (2000).